

Article

A Comprehensive Study on EDFA Characteristics: Temperature Impact

John A. Bebawi ^{1,†}, Ishac Kandas ^{1,2,3,*}, Mohamed A. El-Osairy ¹ and Moustafa H. Aly ^{4,*}

¹ Department of Engineering Mathematics and Physics, Faculty of Engineering, Alexandria University, Alexandria 21544, Egypt; john.aziz1988@yahoo.com (J.A.B.); melosairy@hotmail.com (M.A.E.-O.)

² Center of Smart Nanotechnology and Photonics (CSNP), Smart CI Research Center, Alexandria University, Alexandria 21544, Egypt

³ Kuwait College of Science and Technology (KCST), Doha District, Block4, Safat 13133, Kuwait

⁴ College of Engineering and Technology, Arab Academy for Science, Technology and Maritime Transport, Alexandria 21544, Egypt

* Correspondence: ishac@vt.edu (I.K.); mosaly@aast.edu (M.H.A.)

† These authors contributed equally to this work.

‡ Member of the Optical Society of America (OSA).

Received: 9 August 2018; Accepted: 10 September 2018; Published: 13 September 2018



Abstract: In this paper, a comprehensive study on erbium-doped fiber amplifier (EDFA) characteristics under temperature variation has been performed. The rate and propagation equations that characterize EDFA performance pumped at 980 nm and 1480 nm in the forward direction are solved numerically. The Boltzmann distribution between the pump and the gain wavelength is taken into account, and is found to be effective when pumping only at 1480 nm. In addition, a full comparison between the effect of temperature on some of the EDFA characteristics such as the maximum peak gain, optimum fiber length, saturation input power, and saturation output power has been carried out. The temperature variation in the range from $-40\text{ }^{\circ}\text{C}$ to $+80\text{ }^{\circ}\text{C}$ is taken into account.

Keywords: optical amplifiers; fiber optic amplifiers and oscillators; erbium; pumping; emission; temperature

1. Introduction

In early days, communication systems suffered from many limiting factors concerning the permitted transmission distances due to the absorption mechanisms inside the fiber [1]. The first applied solution to avoid absorption loss was the use of electrical repeaters to enhance the signal while being transmitted [2]. The main drawback was the need to use optoelectronic (O/E) and electrooptical (E/O) energy converters, which caused the system to be more complicated. Additionally, cost is increased and slow rates are gained [1,2]. Optical amplifiers were developed in the early 1980s, but were used commercially in the 1990s [1]. They represented the solution thanks to introducing a fully optical system [3]. The common types of optical amplifiers are: semiconductor optical amplifier (SOA) [4–6], Raman amplifier (RA) [6,7] and rare-earth doped fiber amplifier (DFA) [4,6].

Rare-earth DFAs have some advantages over SOAs due to their lower noise and higher gain, while they are also advantageous compared to RAs for their lower cost and higher pump power utilization. Also, amplification using DFAs can cover a wide range of wavelengths of input signals. The range could be from visible to infrared depending on the rare-earth material used as a dopant [2,8]. The most frequently used rare-earth material is the erbium (Er^{+3}) [2,3]. This is due to its capability of operating in the broad range of the third transmission window at 1550 nm, which is characterized by its minimum attenuation [9]. The amplifier in this case is called an erbium-doped fiber amplifier

(EDFA). Other rare-earth elements are also used in several applications such as: lanthanum (La) in the improvement of the microstructure and mechanical properties of some aluminum alloys [10], and ytterbium (Yb) in signal amplification in the 975–1200 nm range [11,12].

An EDFA pumping laser wavelength should be 980 nm or 1480 nm [3,13]. However, the 1480 nm has also some advantages over the 980 nm pumping wavelength. It is less affected by the so-called excited state absorption (ESA) that results from various transitions to upper energy levels in case of strong pumping schemes [14,15], and affects the pump absorption along the fiber [16]. In addition, according to Cüneyt Berkdemir et al. [14], although the 980-nm pumping affords a weaker dependence of the performance of EDFA on temperature than that for 1480-nm pumping, a more effective performance of EDFA at the pumping wavelength of 1480 nm as compared to the 980 nm is obtained for a wide range of temperature and high-pump powers. Other pumping wavelengths are also available such as: 510 nm, 532 nm, 665 nm, and 810 nm. However, these wavelengths suffer from the ESA. Different pumping configurations can be used such as forward, backward, or even bi-directional configuration [17]. Modeling EDFA gain and its characteristics has been studied in the literature, in addition to gain temperature dependency. However, the main concern was only dedicated to the gain variation with temperature [12,18–20]. Another drawback is the use of complicated methods in some of these studies [20,21]. Also, the EDFA gain dependency on temperature has been used in some sensing applications [22]. Despite this, to the best of our knowledge, no complete and comprehensive investigation has been driven regarding the EDFA characteristics' dependency on temperature.

The aim of this work is to present a simple analytical model to follow and use to fully study the temperature impact on EDFA gain in case of 1480-nm pumping schema. The temperature range under study is $-40\text{ }^{\circ}\text{C}$ to $+80\text{ }^{\circ}\text{C}$. Here, the solutions are calculated numerically, and summations replace the integrals of the previous work [14,23]. In addition, previous work has focused on gain temperature dependency. In our work, the investigation of temperature effect is extended to include the effect of more EDFA parameters such as the maximum peak gain, optimum fiber length, saturation output signal power, and saturation pump power.

This paper is organized as follows. Section 2 introduces the simple proposed analytical model. The obtained results following this model are presented and discussed in Section 3. This is followed by the main conclusions in Section 4.

2. Analytical Model

In EDFA, the signal to be amplified and the pump signal are multiplexed together into the doped fiber. The EDFA amplification is achieved by the stimulated emission of the input signal photons. In addition, spontaneous emission takes place and reduces the efficiency of light signal amplification through amplified spontaneous emission (ASE). Concerning the pumping wavelength, a three-energy level model is used for 980-nm pumping as in Figure 1, while a two-level model can be used for 1480-nm pumping [2,3,23]. In Figure 1, R_{13} and R_{31} represent, respectively, the pumping and stimulated emission rates between levels 1 and 3. W_{12} and W_{21} represent the stimulated absorption and stimulated emission rates between levels 1 and 2, respectively. A_{21}^R is the assumed dominant radiative spontaneous decay rate from level 2 to level 1 [3]. This radiative decay is the reciprocal of fluorescence life time (τ). A_{32}^{NR} represents the assumed dominant non-radiative spontaneous decay rate from level 3 to level 2 [3]. It can also be noted from the figure that the ground state $^4I_{15/2}$ is a manifold consisting of eight sublevels of energy E_{1j} ; meanwhile, the meta-stable state $^4I_{13/2}$ is a manifold consisting of seven sublevels of energy E_{2j} [24], where the superscript j refers to the sublevel order.

Complete population inversion can be achieved with 980-nm pumping, while incomplete inverted population is noticed in the case of 1480-nm pumping [14].

To study the EDFA amplification through the fiber length in the signal direction of propagation, two sets of equations are needed: the rate equations and the propagation equations. All of these equations depend on the absorption and emission cross-sections of the dopant, which is erbium in our study.

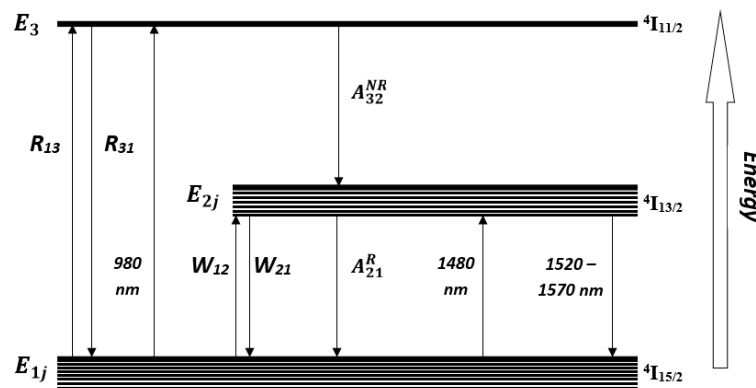


Figure 1. Energy level illustration for Er-doped silica fiber.

2.1. Absorption and Emission Cross-Sections

The absorption or emission cross-section is a material characteristic that determines the rate of a transition such as absorption or stimulated emission transition. An accurate determination of absorption and emission cross-sections is necessary in order to get an exact solution for both rate and propagation equations. Usually, the absorption cross-section is measured experimentally using commercial spectrophotometers [8,25]. Many techniques have been raised in order to get a complete representation of both cross-sections, such as: Ladenburg–Fuchtbauer relation [26], and McCumber relation [8,27]. The McCumber relation is usually used to relate the absorption and emission cross-sections due to its great validity and simplicity [2,28]. The McCumber relation takes the form [27]:

$$\sigma_e(\lambda) = \sigma_a(\lambda)e^{\frac{\epsilon - h\nu}{k_B T}} \tag{1}$$

where $\sigma_e(\lambda)$ is the emission cross-section, $\sigma_a(\lambda)$ is the absorption cross-section, k_B is Boltzmann’s constant, T is the absolute temperature, h is Planck’s constant, ν represents the operating frequency, and ϵ is the net free energy required to excite one Er^{+3} ion from the $4I_{15/2}$ to the $4I_{13/2}$ state at temperature T .

It can be noted that at only one frequency ($\nu = \epsilon/h$), the two spectra of the cross-sections are the same. At higher frequencies (shorter wavelengths), the absorption cross-section is larger, while at lower frequencies (longer wavelengths), the emission cross-section is larger [8].

2.2. Rate Equations

We take into account the three-level model, as shown in Figure 1. The population density in energy level 1 (ground state), energy level 2 (metastable state), and energy level 3 (pumping state) are N_1 , N_2 , and N_3 , respectively.

The system of differential rate equations is driven as follows [2,3,29]:

$$\frac{dN_1}{dt} = -R_{13}N_1 + R_{31}N_3 - W_{12}N_1 + W_{21}N_2 + A_{21}N_2 \tag{2a}$$

$$\frac{dN_2}{dt} = W_{12}N_1 - W_{21}N_2 - A_{21}N_2 + A_{32}N_3 \tag{2b}$$

$$\frac{dN_3}{dt} = R_{13}N_1 - R_{31}N_3 - A_{32}N_3 \tag{2c}$$

Assuming the steady-state condition ($\frac{dN_1}{dt} = \frac{dN_2}{dt} = \frac{dN_3}{dt} = 0$) and solving the three differential rate equations yields [3,30]:

$$N_2 = \frac{R_{13} + W_{12}}{\frac{1}{\tau} + R_{13} + R_{31} + W_{12} + W_{21}} N \tag{3a}$$

where N represents the total E_r^{+3} ion density. Then:

$$N_1 = N - N_2 \tag{3b}$$

where N_3 is negligible due to the very fast life time for the energy level 3 ($\sim 1 \mu s$) as compared to that of the energy level 2 ($\sim 10 ms$) [2,3,16].

The rates W_{12} , W_{21} , R_{13} , and R_{31} are related to the absorption and emission cross-sections through the following equations [3,29,30]:

$$W_{12} = \frac{\sigma_s^a \Gamma_s (P_s + P_{ASE}^+ + P_{ASE}^-)}{h\nu_s A_{eff}} \tag{4a}$$

$$W_{21} = \frac{\sigma_s^e \Gamma_s (P_s + P_{ASE}^+ + P_{ASE}^-)}{h\nu_s A_{eff}} \tag{4b}$$

$$R_{13} = \frac{\sigma_p^a \Gamma_p P_p}{h\nu_p A_{eff}} \tag{4c}$$

$$R_{31} = \frac{\sigma_p^e \Gamma_p P_p}{h\nu_p A_{eff}} \tag{4d}$$

where h is Planck’s constant, and A_{eff} is the fibereffective area doped with E_r^{+3} ions. P_s and P_p are, respectively, the signal power transmitted through the fiber and the pump power driven into the fiber along its length. P_{ASE}^+ and P_{ASE}^- represent the amplified spontaneous emission (ASE) power in both forward and backward directions, respectively. ν_s and ν_p represent the signal and pump frequencies, respectively. σ_s^a , σ_s^e , σ_p^a and σ_p^e represent the absorption (a) and emission (e) cross-sections at the signal (s) and pump (p) wavelengths, respectively.

The overlap factors at the signal and pump wavelength are, respectively, Γ_s and Γ_p . They can be obtained through using the following equation [3]:

$$\Gamma(\lambda) = 1 - e^{-\frac{2b^2}{w}} \tag{5}$$

where b represents the erbium ion E_r^{+3} doping radius, and w represents the mode radius, which can be calculated using several models. The model used here is the Myslinski one [31]:

$$w = a \left(0.761 + \frac{1.237}{V^{1.5}} + \frac{1.429}{V^6} \right) \tag{6}$$

where a is the fiber core radius, and V is the normalized frequency, which is defined as:

$$V = \frac{2\pi a}{\lambda} NA \tag{7}$$

where λ is the operating wavelength and NA is the numerical aperture.

In case of multichannel signals, the final form of the rate equations should be changed to be [2]:

$$N_2 = \frac{\frac{\sigma_p^a \Gamma_p}{h\nu_p A_{eff}} P_p + \sum_{i=1}^{s_i} \frac{\sigma_{si}^a \Gamma_{si}}{h\nu_{si} A_{eff}} (P_{si} + P_{ASE}^+ + P_{ASE}^-)}{\frac{1}{\tau} + \frac{(\sigma_p^a + \sigma_p^e) \Gamma_p}{h\nu_p A_{eff}} P_p + \sum_{i=1}^{s_i} \frac{(\sigma_{si}^a + \sigma_{si}^e) \Gamma_{si}}{h\nu_{si} A_{eff}} (P_{si} + P_{ASE}^+ + P_{ASE}^-)} \tag{8}$$

Equation (8) is used in case of studying the change of the parameter under test with the signal wavelength. In this case, several input signals with different wavelengths are multiplexed together within the same fiber.

It is worthy to mention that in case of temperature variation, modified rate equations should be used that depend on the Boltzmann distribution law [32]. Its effect is very small in the case of

980-nm pumping and can be neglected, while it causes a remarkable change in the case of 1480-nm pumping [14]. Therefore, it will be taken into consideration when studying the propagation equations.

2.3. Propagation Equation

The propagation equations are studied here in order to represent the full distribution of each signal while propagating through the fiber. Based on the Giles and Desurvire model [2,33] and by using the modified rate equations, the propagation equations are [14,23]:

$$\frac{dP_p}{dz} = P_p \Gamma_p (\beta \sigma_p^e N_2 - \sigma_p^a N_1) - \alpha_p P_p \tag{9a}$$

$$\frac{dP_s}{dz} = P_s \Gamma_s (\sigma_s^e N_2 - \sigma_s^a N_1) - \alpha_s P_s \tag{9b}$$

$$\frac{dP_{ASE}^\pm}{dz} = \pm P_{ASE}^\pm \Gamma_s (\sigma_s^e N_2 - \sigma_s^a N_1) \pm 2 \sigma_s^e N_2 \Gamma_s P_{ASE}^\pm \Delta\nu \mp \alpha_s P_{ASE}^\pm \tag{9c}$$

where z is the propagation direction through the fiber, and $\Delta\nu$ is the homogeneous bandwidth. α_s and α_p are the fiber loss for the signal and pump, respectively. Both losses can be neglected in the case of short fiber, which is our case [2]. Here, β is defined as the Boltzmann factor. It is the only factor, in addition to the emission and absorption cross-sections, that depends on temperature. It can be obtained from the Boltzmann distribution law [32]:

$$\beta = \exp\left(-\frac{\varepsilon E_2}{k_B T}\right) \tag{10}$$

where ΔE_2 ($E_{2+} - E_{2-}$) represents the difference in energy between the upper and the lower sublevels' energies E_{2+} and E_{2-} , respectively [3].

2.4. Gain and Optimum Fiber Length Calculation

EDFA gain (G) along the fiber length (L) is defined as the ratio of the signal output power at the fiber end ($z = L$) to the input signal power driven inside the fiber ($z = 0$), i.e.,

$$G = \frac{P_s(L)}{P_s(0)} \tag{11}$$

The optimum fiber length is defined as the typical fiber length designed in order to get maximum EDFA gain. It is important for evaluating the EDFA performance, and can be obtained using the model proposed by Desurvire, Nusinsky et al., and Lin et al. [3,21,30]. Another simpler model that fits our simulation parameters and results in a complete accordance between analytical and graphical results is [15]:

$$\left[G|_{L_{opt}}\right]^{\beta_o} e^{-\beta_o \Gamma_s \sigma_s^e N L_{opt}} = \frac{A_{eff} h \nu_p \sigma_s^a}{\tau P_p(0) \Gamma_p \sigma_p^a \sigma_s^e} \tag{12a}$$

where:

$$\beta_o = \frac{\Gamma_p \sigma_p^a}{\Gamma_s (\sigma_s^e + \sigma_s^a)} \tag{12b}$$

3. Results and Discussion

A variety of evaluation parameters such as maximum peak gain, optimum fiber length, L_{opt} , saturation signal power, P_{sat}^s , and saturation pump power, P_{sat}^p , are investigated. Each parameter is tested for several other related parameters such as the change of the driven input signal power, P_s^{in} , fiber length, L , and driven pump power, P_p^{in} . The effect of temperature on each parameter is then tested, and the results are graphically displayed.

In this paper, all of the investigations are made on an Al/P-Silica EDFA at room temperature (27 °C) [34] using the parameters shown in Table 1 [21]. To calculate the EDFA gain, first, the rate equations, Equations (3)–(5), are solved together. The effect of temperature on cross-sections is carried out using the McCumber relation, Equation (1), and the overlap factor is calculated from Equations (5)–(7). Then, the propagation equations are solved together from Equation (9) using a forward explicit Euler’s method. Here, the effect of temperature is presented in this set of equations through both the cross-sections and the Boltzmann factor. For the sake of comparison, we have chosen the temperature range from -40 °C to $+80$ °C such as in the work of Kentchou et al., Bolshtyansky et al., Berkdemir et al., Öszoý et al., and Husein at al. [19,20,23,35,36]. The value of ΔE_2 was chosen to be 200 cm^{-1} for simplicity [14]. Some boundary conditions are taken into account. First, we consider that the amplified spontaneous emission (ASE) power in the forward direction, P_{ASE}^+ , is zero at the entry of the EDFA. Also, ASE power in the backward direction, P_{ASE}^- , is considered to be zero at its end.

Table 1. Al/P-Silica erbium-doped fiber amplifier (EDFA) parameters used in simulation [21].

Parameter	Symbol	Value
Core effective area	A_{eff}	$1.96 \times 10^{-11} \text{ m}^2$
E_r^{+3} ion doping radius	B	2.5 μm
Pump wavelength	λ_p	1480 nm
Signal wavelength	λ_s	1532 nm
Pump absorption cross-section	σ_p^a	$2.4312 \times 10^{-25} \text{ m}^2$
Pump emission cross-section	σ_p^e	$0.7164 \times 10^{-25} \text{ m}^2$
Signal absorption cross-section	σ_s^a	$6.2778 \times 10^{-25} \text{ m}^2$
Signal emission cross-section	σ_s^e	$5.5644 \times 10^{-25} \text{ m}^2$
Fluorescence life time	τ	10.8 ms
Total E_r^{+3} ion density	N	$1 \times 10^{25} \text{ ion/m}^3$
Core refractive index	N	1.5
Numerical aperture	NA	0.18

The values of all of the needed parameters in the simulation are shown in Table 1. The used absorption and emission cross-sections at room temperature are extracted from the work of Miniscalco [34], and are typical for Al/P-Silica erbium-doped glasses.

We validate the accuracy of the used analytical model in our work to the study concerning the optimum fiber length, which was calculated already and introduced by Geguo et al. [15]. The procedure is accomplished by setting $\beta = 1$, and the obtained values are found in a complete agreement with that mentioned and simulated in Figure 5 in the work of Geguo et al. [15]. Another check was accomplished using the given parameters by Nusinsky [21], where again a fair agreement was found between the obtained results and already simulated results in Figure 2 by Nusinsky [21].

3.1. Emission Cross-Section Variation with Temperature

In order to investigate the influence of temperature on the emission cross-section, the wavelength at which the two cross-sections spectrums are equal is of great importance. From the experimental work, this wavelength was found to be 1537.9 nm [34] and the net free energy, ε required to excite one E_r^{+3} ion from the $^4I_{15/2}$ to the $^4I_{13/2}$ has been calculated from its experimental definition ($\nu = \varepsilon/h$) to be 0.8078 eV. Finally, the McCumber relation has been applied to the emission cross-section, and its variation with temperature in the range from -40 °C to $+80$ °C is shown in Figure 2. A small variation in gain amplitude with a slight variation in temperature is noticed, but with no shift toward longer or shorter wavelengths. Hence, it can be revealed that the window at which the signal is

amplified is not affected by the temperature variation. Another observation from Figure 2 is that the wavelength at which all of the emission cross-section curves meet the absorption cross-section curve is 1537.9 nm. At shorter wavelengths, an increase in temperature causes an increase in the value of the emission cross-section. At longer wavelengths, the effect is opposite, and the emission cross-section decreases with temperature. Our results are found to be in a good agreement with those obtained by J. Kemtchou et al. [19].

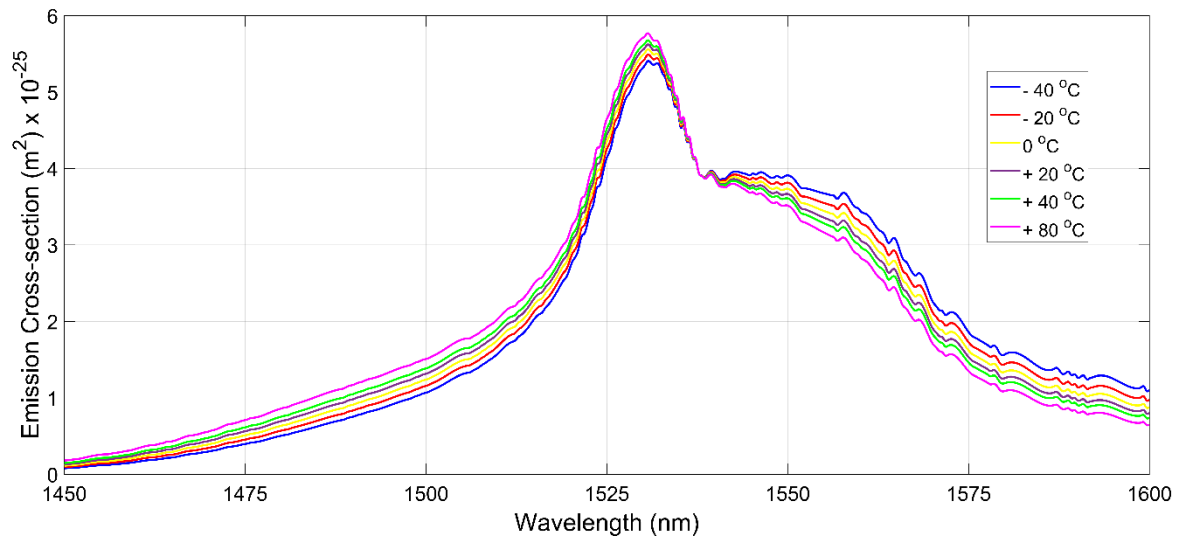


Figure 2. Emission cross-sections change wavelengths at different temperatures.

3.2. Temperature Effect on EDFA Gain

The EDFA gain is displayed, in Figure 3, versus the input signal wavelength at $-40\text{ }^{\circ}\text{C}$ and $+80\text{ }^{\circ}\text{C}$ for the two different pumping wavelengths. The fiber length is chosen to be 5 m. The input pump and signal power are 200 mW, and 10 μW , respectively. As expected, in both parts (a) and (b), the maximum gain is achieved at $\sim 1531\text{ nm}$, which corresponds to the wavelength of the maximum emission cross-section.

The effect of β and its variation with temperature is also considered in Figure 3, for both pumping cases. Figure 3a shows that β has no effect in the case of 980-nm pumping. However, in the case of 1480-nm pumping, it has a noticeable effect, as depicted from Figure 3b. This agrees with the results obtained by Cüneyt Berkdemir et al. [14]. Noting that, neglecting the β effect leads to a false increase in the gain value by around 4 dB at a signal wavelength of 1531 nm for both temperature values. It is also noted that the effect of β is neglected in the case of 1480-nm pumping at longer signal wavelengths, $\sim 1600\text{ nm}$, which is out of the scope of our study.

It is worthy to study the significant impact of temperature on the EDFA gain. Below a certain wavelength, the increase in temperature has a positive influence on the gain. On the other hand, after this wavelength, the effect is negative, and a decrease in gain is observed. This wavelength is 1542 nm in the case of the 980-nm pumping schema, while its value is 1535 nm in the 1480-nm pumping case.

3.3. Maximum Gain Variation with Temperature

The EDFA gain variation with input signal wavelength that is represented in Figure 3 showed two different peaks. One narrow peak is located around 1530 nm, while another wider peak is located at around 1550 nm. In case of a 3-m Al/P-Silica EDFA with the input and pump powers of 10 μW and 80 mW, respectively, the maximum of the two peaks is the narrow one located at exactly 1532 nm. Its variation with the operating temperature is depicted in Figure 4.

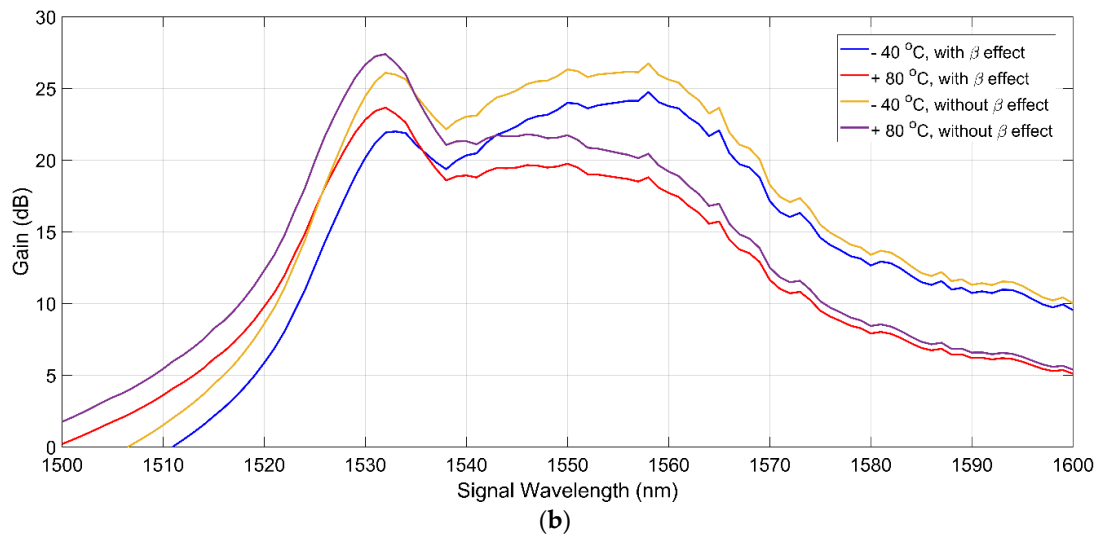
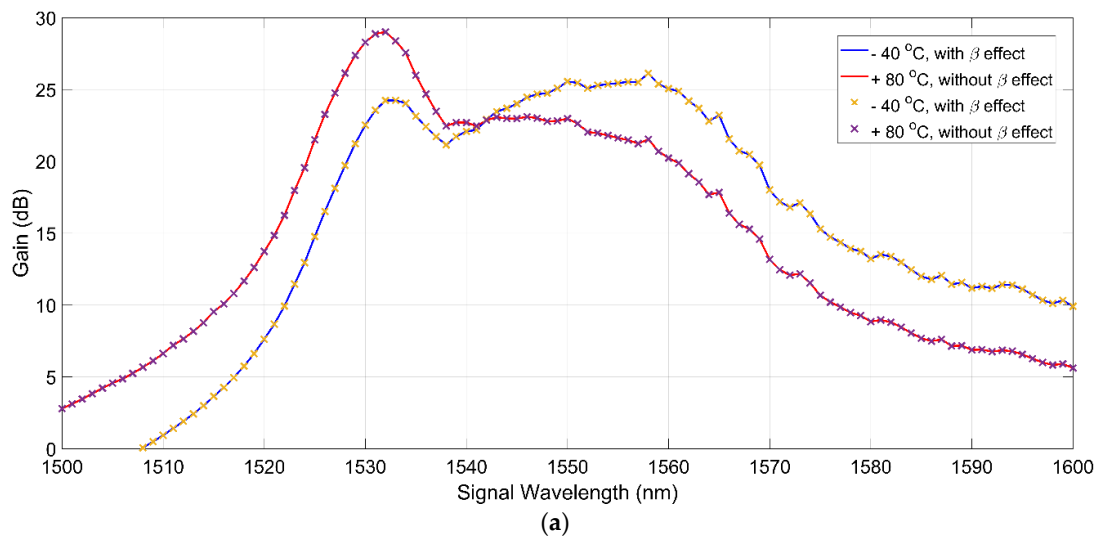


Figure 3. Gain variation with signal wavelength at different temperatures when pumped with (a) 980 nm and (b) 1480 nm.

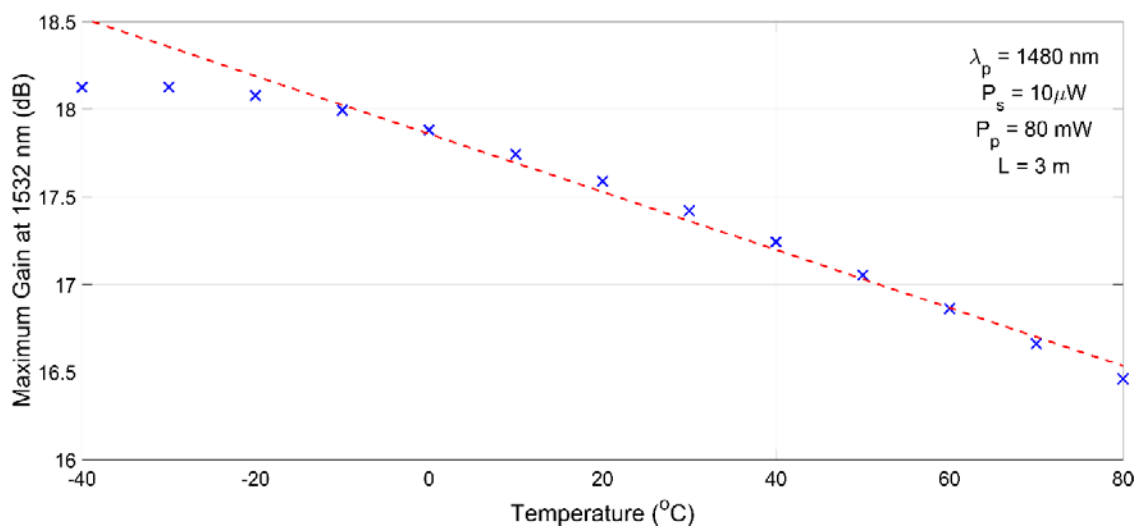


Figure 4. Maximum gain variation with temperature compared to a linear best fit (dotted red).

From Figure 4, it can be noted that the maximum gain value at the 1532-nm input signal wavelength shows a nearly linear decrease in its value with the increase in the surrounding temperature while working at an environmental temperature higher than $-20\text{ }^{\circ}\text{C}$. This linear behavior is also proved through the linear best fitting simulated in the figure by the dotted red line. It is worthy to mention that changing any of the EDFA operating parameters will affect the maximum gain variation with temperature.

3.4. Optimum Fiber Length Variation with Temperature

The optimum fiber length, L_{opt} , investigation shows its dependency on several parameters such as input signal power and input pump power as follows.

3.4.1. Dependency of L_{opt} on Input Signal Power

The effect of input signal power on L_{opt} variation with temperature is studied in Figure 5. Three different input signal powers are chosen: $1\text{ }\mu\text{W}$, $5\text{ }\mu\text{W}$, and $10\text{ }\mu\text{W}$. The corresponding optimum fiber length is calculated using Equation (12) for an input pump power of 200 mW . For the case of the maximum gain amplification channel located at 1532 nm and pumped using a pump wavelength of 1480 nm , the signal and pump overlap factors are calculated using Equations (5)–(7), and are found to be 0.6986 and 0.7165 , respectively. A decrease in the value of the optimum fiber length with the input signal power is observed. This is needed in the fiber design; otherwise, no maximum gain could be obtained. This result is in fair agreement with both the numerical and analytical solutions of Inna Nusinsky et al. [21].

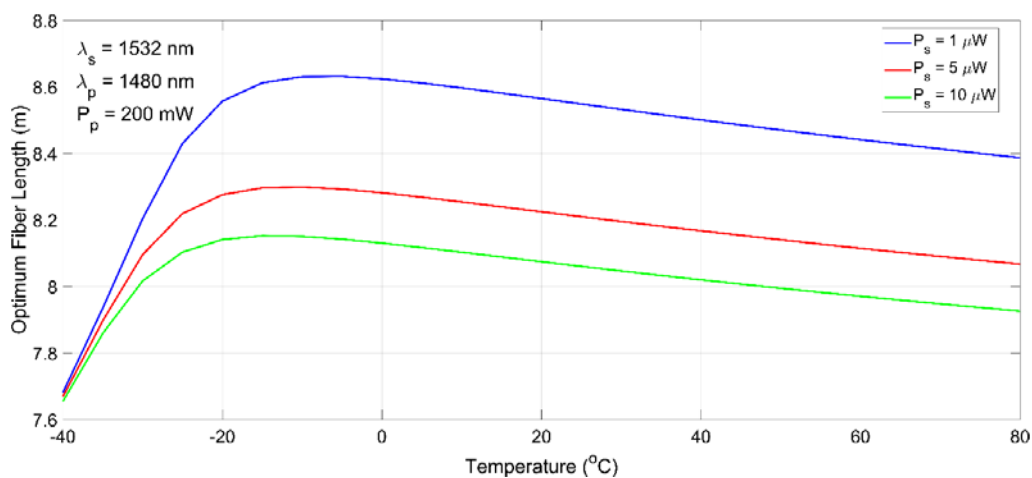


Figure 5. Variation of L_{opt} with temperature for three different input signal powers: $1\text{ }\mu\text{W}$, $5\text{ }\mu\text{W}$, and $10\text{ }\mu\text{W}$.

It is also noticeable that while changing the environmental temperature, there is a certain temperature value at which the value of L_{opt} is maximized. At lower temperature values, the L_{opt} value increases with the increase in temperature, while an opposite behavior occurs at higher temperature values. Concerning this limiting temperature at which L_{opt} is at its maximum, its value decreases with the increase in the driven input signal power, as illustrated in Figure 5.

3.4.2. Dependency of L_{opt} on Input Pump Power

The effect of input pump power on L_{opt} variation with temperature is studied in Figure 6. Three different input pump powers are chosen: 50 mW , 100 mW , and 200 mW , while the corresponding L_{opt} is calculated using Equation (12). To accomplish the simulation, an input signal power of $10\text{ }\mu\text{W}$ is used. An increase in L_{opt} is noticed with increasing input pump power, which supports the best fiber length design that is needed to acquire the highest possible gain.

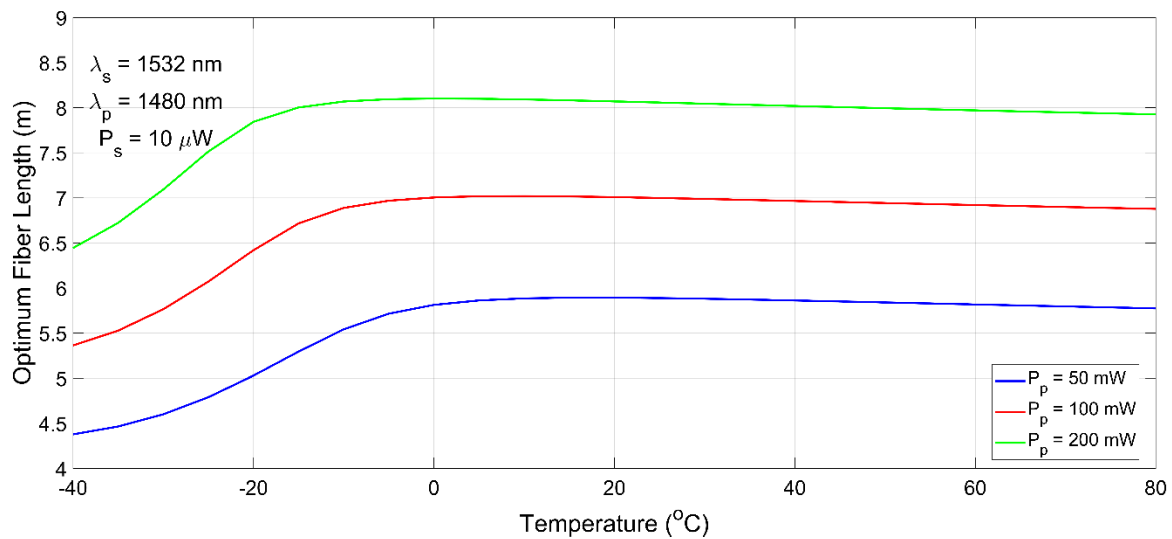


Figure 6. Variation of L_{opt} with input pump power using $P_s = 10 \mu\text{W}$ at different temperatures with $\lambda_p = 1480$ nm.

Also, it is noticed that a certain temperature value exists at which the value of L_{opt} is maximized, as already stated in the last section. At lower temperature values, the value of L_{opt} increases with the temperature increase. However, at higher temperature values, a decrease in the corresponding value of L_{opt} is noticed. Concerning this limiting temperature at which L_{opt} is at its maximum, its value decreases with the increase in the driven input pump power, as illustrated in Figure 6.

3.5. Saturation Signal Power Variation with Temperature

The study of the saturation signal power P_s^{sat} is of great importance in order to have a complete overview concerning the maximum possible input signal power that could be driven to the fiber without affecting its output gain. The saturation signal power could be defined as the input signal power at which the gain has been reduced by 3 dB of its small-signal gain. From previous studies [2,3], increasing the input signal power will push into the saturation region because, in this case, the number of photons of the input signal will be higher than the number of carriers in the meta-stable state. The saturation signal power investigation shows its dependency on the input pump power. This will be explained as follows.

To calculate the saturation signal power, the gain versus the input signal power should be driven first for each parameter that needs to be studied. The input signal power related to a value of gain lower than the maximum gain value by 3 dB represents the saturation signal power. The gain versus the input signal power is depicted in Figure 7. The EDFA length is 2 m, and the input pump power is 200 mW.

The effect of temperature has been studied in the range from -40 °C to $+80$ °C. It is worthy to choose the fiber length to be L_{opt} . It could easily be calculated to be 6.86 m using Equation (12) in which the simulation data for P_s , P_p , λ_s and T have the following values: 0.05 mW, 200 mW, 1530 nm, and 300 K, respectively. This choice will afford a high gain of ~ 36.9 dB in the case of a very low input signal power at -40 °C. However, this length will not provide gain saturation in the case of a low-input power signal, and hence the concept of calculating P_s^{sat} will not be accomplished, which is why we have chosen the fiber length to be 2 m. Another important observation is that the gain versus the input signal power variation with temperature is clearer in the case of 1480-nm pumping rather than 980-nm pumping, because this last case is less sensitive to temperature variation [13]. This result led Paul Kai Nu Ko et al. [22] to use a laser with a wavelength of 1480 nm in their sensing application using EDFA.

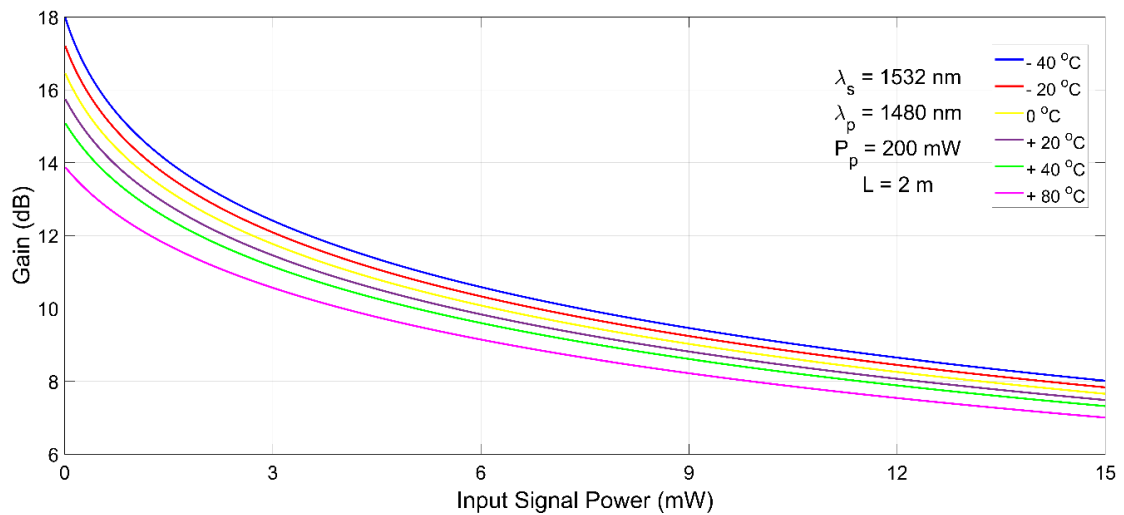


Figure 7. Gain versus input signal power.

Figure 8 represents the effect of changing the pump power on the saturation signal power variation with temperature. The fiber length is chosen to be 2 m, and the temperature is in the range from $-40\text{ }^{\circ}\text{C}$ to $+80\text{ }^{\circ}\text{C}$. An increase in the value of the saturation signal power with temperature is noticeable. Hence, working at higher temperature ranges will afford higher opportunities to amplify input signals while conserving a flat output amplified signal. Also, one can notice the increase in the saturation pump power due to the temperature increase with the increase of the driven signal power in the case of the 1480-nm pumping.

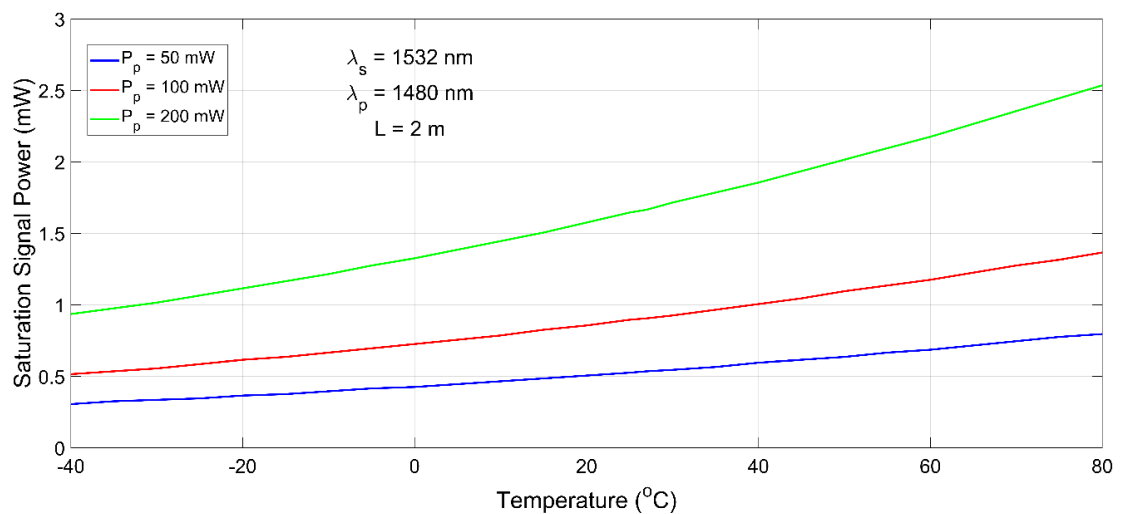


Figure 8. Saturation signal power variation with temperature.

3.6. Saturation Pump Power Variation with Temperature

The saturation pump power is another important factor in the study of the fiber performance in order to have a complete overview concerning the minimum required pump power to have an optically amplified signal. It could be defined as the input pump power at which the gain has been reduced by 3 dB of its saturation gain value. From previous studies [2,3], increasing the input pump power will increase the number of carriers in the meta-stable state, and this continues until all of the carriers in the ground state are stimulated into the meta-stable state. At this level, any increase in the number of carriers in the meta-stable state will not affect the amplification, and the saturation region is reached. The saturation pump power investigation shows its dependency on several parameters, such as: input signal power and signal wavelength, as follows.

The gain versus input pump power should be obtained first at different temperatures using the 1480-nm pumping wavelength, as shown in Figure 9. The EDFA length is 4 m, and the input signal power is 10 μ W. The effect of temperature is studied in the range from $-40\text{ }^{\circ}\text{C}$ to $+80\text{ }^{\circ}\text{C}$. Again, the higher temperature sensitivity of the 1480-nm pumping compared to the 980-nm pumping regime is revealed when comparing the gain versus input pump power variation with temperature for both cases, as previously stated in Section 3.5.

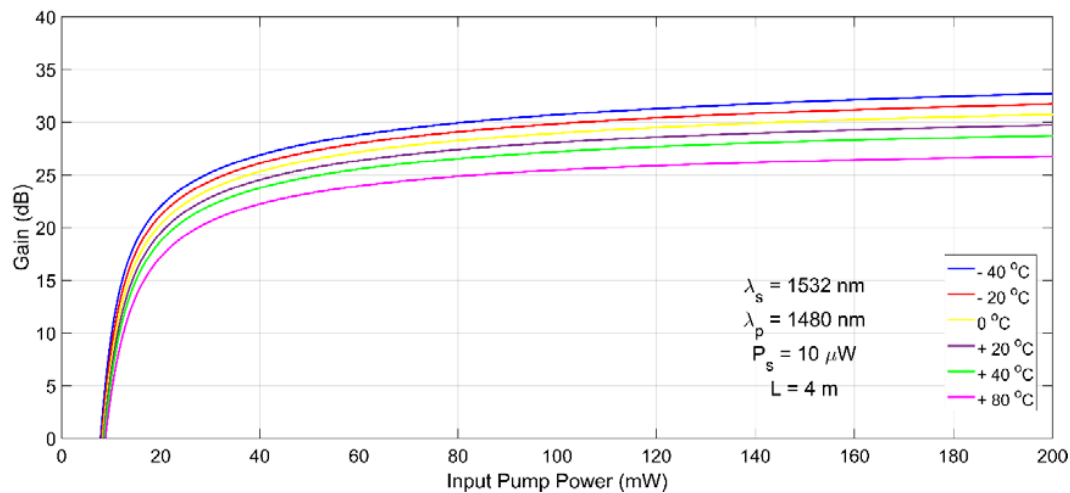


Figure 9. Gain versus input pump power.

The effect of the input signal power on the saturation pump power variation with temperature is displayed in Figure 10. A 4-m fiber length is pumped using an 1480-nm laser beam at a temperature range from $-40\text{ }^{\circ}\text{C}$ to $+80\text{ }^{\circ}\text{C}$. A notable decrease is observed in the value of the saturation pump power with the increase of the temperature. Also, one can notice the negative impact of temperature on the saturation pump power variation with the increase of the driven signal power in the 1480-nm pumping case.

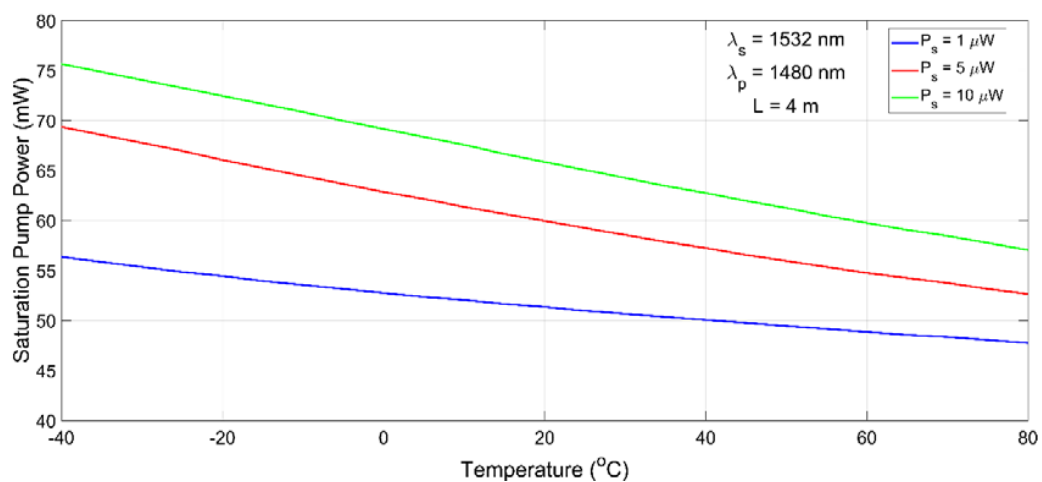


Figure 10. Saturation pump power variation with temperature.

4. Conclusions

In this study, the rate and propagation equations that characterize EDFA performance pumped at both 980 nm and 1480 nm in the forward direction are solved numerically, and the obtained results are displayed graphically. The main EDFA parameters are investigated in the temperature range from $-40\text{ }^{\circ}\text{C}$ to $+80\text{ }^{\circ}\text{C}$. A 1480-nm pumping wavelength is chosen for its lower neglected ESA and its effective performance as compared to other pumping schemes. The obtained results showed a small

but effective variation of the emission cross-section with temperature. The effect of the Boltzmann factor and its variation with temperature is taken into consideration, and is found to be effective only in the case of 1480 nm. In general, the obtained results imply a better gain performance at higher temperatures. The maximum gain is found to be decreased linearly for temperatures greater than $-20\text{ }^{\circ}\text{C}$. Regarding the optimum fiber length, its variation with temperature shows a maximum value at a certain temperature while fixing either the input signal power or pump power. The value of this temperature decreases with the increase of the input signal power and the pump power. The saturation signal power increases, and the saturation pump power decreases with the temperature increase.

Author Contributions: Conceptualization, I.K. and M.H.A.; Methodology, J.A.B.; Software, J.A.B.; Validation, J.A.B., I.K. and M.H.A.; Formal Analysis, J.A.B.; Investigation, J.A.B.; Resources, I.K.; Data Curation, J.A.B.; Writing-Original Draft Preparation, J.A.B.; Writing-Review & Editing, I.K., M.H.A. and M.A.E-O.; Visualization, J.A.B. and I.K.; Supervision, I.K., M.H.A. and M.A.E-O.; Project Administration, M.H.A. and M.A.E-O.

Funding: This research received no external funding.

Conflicts of Interest: The authors declare no conflict of interest.

References

1. Agrawal, G.P. *Fiber-Optic Communication Systems*, 3rd ed.; John Wiley & Sons: New York, NY, USA, 2002; ISBN 0-471-22114-7.
2. Becker, P.C.; Olsson, N.A.; Simpson, J.R. *Erbium-Doped Fiber Amplifier: Fundamental and Technologies*, 4th ed.; Academic Press: New York, NY, USA, 1997; ISBN 0-12-084590-3.
3. Desurvire, E. *Erbium-Doped Fiber Amplifier: Principles and Applications*, 1st ed.; John Wiley & Sons: New York, NY, USA, 1994; ISBN 0-471-58977-2.
4. Choi, B.-H.; Lee, S.S. Input power dynamic range analysis of SOA and EDFA link extenders on TDM-PON systems without burst effect control. *J. Opt. Commun.* **2013**, *286*, 187–191. [[CrossRef](#)]
5. Zhou, P.; Zhan, W.; Mukaikubo, M.; Nakano, Y.; Tanemura, T. Reflective semiconductor optical amplifier with segmented electrodes for high-speed self-seeded colorless transmitter. *J. Opt. Express* **2017**, *25*, 28547–28555. [[CrossRef](#)]
6. Singh, S.; Singh, A.; Kaler, R.S. Performance evaluation of EDFA, RAMAN and SOA optical amplifier for WDM systems. *Optik* **2013**, *124*, 95–101. [[CrossRef](#)]
7. Barth, I.; Fisch, N.J. Multifrequencyraman amplifiers. *J. Phys. Rev. E* **2018**, *97*, 1–6. [[CrossRef](#)] [[PubMed](#)]
8. Miniscalco, W.J. Optical and electronic properties of rare earth ions in glasses. In *Rare-Earth-Doped Fiber Lasers and Amplifiers*; Digonnet, M.J.F., Ed.; Marcel Dekker: New York, NY, USA, 2001; pp. 17–105, ISBN 0-8247-0458-4.
9. Desurvire, E.; Simpson, J.R. Amplification of spontaneous emission in erbium-doped single-mode fibers. *J. Lightw. Technol.* **1989**, *7*, 835–845. [[CrossRef](#)]
10. Liu, W.; Yan, H.; Zhu, J.-B. Effect of the addition of rare earth element La on the tribological behaviour of AlSi5Cu1Mg alloy. *J. Appl. Sci.* **2018**, *8*, 163. [[CrossRef](#)]
11. Jauregui, C.; Otto, H.-J.; Breikopf, S.; Limpert, J.; Tünnermann, A. Optimizing high-power Yb-doped fiber amplifier systems in the presence of transverse mode instabilities. *Opt. Express* **2016**, *24*, 7879–7892. [[CrossRef](#)] [[PubMed](#)]
12. Jayarajan, P.; Kuppasamy, P.G.; Sundararajan, T.V.P.; Thiyagupriyadharsan, M.R.; Ahamed Yasar, Z.; Maheswar, R.; Amiri Iraj, S. Analysis of temperature based power spectrum in EDFA and YDFA with different pump power for THz applications. *J. Results Phys.* **2018**, *10*, 160–163. [[CrossRef](#)]
13. Yamada, M.; Shimizu, M.; Horiguchi, M.; Okayasu, M. Temperature dependence of signal gain in Er³⁺-doped optical fiber amplifiers. *IEEE J. Quantum Electron.* **1992**, *28*, 640–649. [[CrossRef](#)]
14. Berkdemir, C.; Öszo, S. An investigation of the temperature dependency of the relative population inversion and the gain in EDFAs by the modified rate equations. *J. Opt. Commun.* **2005**, *254*, 248–255. [[CrossRef](#)]
15. Geguo, D.U.; Guofu, C. Gain performances of 980 nm-pumped erbium-doped fiber amplifiers. *Sci. China Ser. A* **1999**, *42*, 286–292. [[CrossRef](#)]
16. Sun, Y.; Zyskind, J.L.; Srivastava, A.K. Average inversion level, modeling, and physics of erbium-doped fiber amplifiers. *J. Sel. Top. Quantum Electron.* **1997**, *3*, 991–1007. [[CrossRef](#)]

17. Liang, T.-C.; Chen, Y.-K.; Su, J.-H.; Tzeng, W.-H.; Hu, C.; Lin, Y.-T.; Lai, Y.-C. Optimum configuration and design of 1480-nm pumped L-band gain-flattened EDFA using conventional erbium-doped fiber. *J. Opt. Commun.* **2000**, *183*, 51–63. [[CrossRef](#)]
18. Lee, J.H.; Lee, W.J.; Park, N. Comparative study on temperature-dependent multichannel gain and noise figure distortion for 1.48- and 0.98- μm pumped EDFA's. *IEEE Photonics Technol. Lett.* **1998**, *10*, 1721–1723.
19. Kemtchou, J.; Duhamel, M.; Chatton, F.; Georges, T.; Lecoy, P. Comparison of temperature dependences of absorption and emission cross sections in different glass hosts of erbium doped fibers. In *Optical Amplifiers and Their Applications* (p. FAW19); Optical Society of America: Washington, DC, USA, 1996; pp. 126–229, ISBN 1-55752-435-X.
20. Bolshtyansky, M.; Wysocki, P.; Conti, N. Model of temperature dependence for gain shape of erbium-doped fiber amplifier. *J. Lightw. Technol.* **2000**, *18*, 1533–1540. [[CrossRef](#)]
21. Nusinsky, I.; Hardy, A.A. Multichannel amplification in strongly pumped EDFAs. *J. Lightw. Technol.* **2004**, *22*, 1946–1952. [[CrossRef](#)]
22. KO, P.K.N.; Demokan, M.S.; Tam, H. Distributed temperature sensing with erbium-doped fiber amplifiers. *J. Lightw. Technol.* **1996**, *14*, 2236–2245.
23. Berkdemir, C.; Öszoy, S. The temperature dependent performance analysis of EDFAs pumped at 1480 nm: A more accurate propagation equation. *J. Opt. Express* **2005**, *13*, 5179–5185. [[CrossRef](#)]
24. Dignonnet, M.J.F.; Murphy-Chutorian, E.; Falquier, D.G. Fundamental limitations of the McCumber relation applied to Er-doped silica and other amorphous-host lasers. *IEEE J. Quantum Electron.* **2002**, *38*, 1629–1637. [[CrossRef](#)]
25. Miniscalco, W.J.; Andrews, L.J.; Thompson, B.A.; Wei, T.; Hall, B.T. ${}^4\text{I}_{13/2} \leftrightarrow {}^4\text{I}_{15/2}$ emission and absorption cross sections for Er^{3+} doped glasses. In *Tunable Solid State Lasers*; Shand, M.L., Jenssen, H.P., Eds.; Optical Society of America: Falmouth, MA, USA, 1989; Volume 5, pp. 71–83, ISBN 1-55752-111-5.
26. Sandoe, J.N.; Sarkies, P.H.; Parke, S. Variation of Er^{3+} cross section for stimulated emission with glass composition. *J. Phys. D Appl. Phys.* **1972**, *5*, 1788–1799. [[CrossRef](#)]
27. McCumber, D.E. Theory of phonon-terminated optical masers. *Phys. Rev.* **1964**, *134*, A299–A306. [[CrossRef](#)]
28. Martin, R.M.; Quimby, R.S. Experimental evidence of the validity of the McCumber theory relating emission and absorption for rare-earth glasses. *J. Opt. Soc. Am.* **2006**, *23*, 1770–1775. [[CrossRef](#)]
29. Novak, S.; Moesle, A. Analytic model for gain modulation in EDFAs. *J. Lightw. Technol.* **2002**, *20*, 975–985. [[CrossRef](#)]
30. Lin, M.C.; Chi, S. The gain and optimal length in the erbium-doped fiber amplifiers with 1480 nm pumping. *IEEE Photonics Technol. Lett.* **1992**, *4*, 354–356. [[CrossRef](#)]
31. Myslinski, P.; Chrostowski, J. Gaussian-mode radius polynomials for modeling doped fiber amplifiers and lasers. *Microw. Opt. Technol. Lett.* **1996**, *11*, 61–64. [[CrossRef](#)]
32. Yariv, A. *Quantum Electronics*, 3rd ed.; John Wiley & Sons: New York, NY, USA, 1989; ISBN 978-0-471-60997-1.
33. Giles, C.R.; Desurvire, E. Modeling erbium-doped fiber amplifiers. *J. Lightw. Technol.* **1991**, *9*, 271–283. [[CrossRef](#)]
34. Miniscalco, W.J. Erbium doped glasses for fiber amplifiers at 1500 nm. *J. Lightw. Technol.* **1991**, *9*, 234–250. [[CrossRef](#)]
35. Berkdemir, C.; Öszoy, S. On the temperature-dependent gain and noise figure analysis of C-band high-concentration EDFAs with the effect of cooperative upconversion. *J. Lightw. Technol.* **2009**, *27*, 1122–1127. [[CrossRef](#)]
36. Husein, A.H.M.; El-Nahal, F.I. Optimizing the EDFA gain for WDM lightwave system with temperature dependency. *Optik* **2012**, *123*, 586–589. [[CrossRef](#)]

